

This Page Is Inserted by IFW Operations
and is not a part of the Official Record

BEST AVAILABLE IMAGES

Defective images within this document are accurate representations of the original documents submitted by the applicant.

Defects in the images may include (but are not limited to):

- BLACK BORDERS
- TEXT CUT OFF AT TOP, BOTTOM OR SIDES
- FADED TEXT
- ILLEGIBLE TEXT
- SKEWED/SLANTED IMAGES
- COLORED PHOTOS
- BLACK OR VERY BLACK AND WHITE DARK PHOTOS
- GRAY SCALE DOCUMENTS

IMAGES ARE BEST AVAILABLE COPY.

**As rescanning documents *will not* correct images,
please do not report the images to the
Image Problem Mailbox.**

Mammalian MutS homologue 5 is required for chromosome pairing in meiosis

Winfried Edelmann^{1*}, Paula E. Cohen^{2*}, Burkhard Kneitz¹, Nena Winand⁴, Marie Lia³, Joerg Heyer³, Richard Kolodner⁴, Jeffrey W. Pollard² & Raju Kucherlapati³

*These authors contributed equally to this work.

MSH5 (MutS homologue 5) is a member of a family of proteins known to be involved in DNA mismatch repair^{1,2}. Germline mutations in *MSH2*, *MLH1* and *GTBP* (also known as *MSH6*) cause hereditary non-polyposis colon cancer (HNPCC) or Lynch syndrome³⁻⁸. Inactivation of *Msh2*, *Mlh1*, *Gtnbp* (also known as *Msh6*) or *Pms2* in mice leads to hereditary predisposition to intestinal and other cancers⁹⁻¹⁴. Early studies in yeast revealed a role for some of these proteins, including Msh5, in meiosis¹⁵⁻¹⁷. Gene targeting studies in mice confirmed roles for *Mlh1* and *Pms2* in mammalian meiosis^{12-14,18}. To assess the role of Msh5 in mammals, we generated and characterized mice with a null mutation in *Msh5*. *Msh5*^{-/-} mice are viable but sterile. Meiosis in these mice is affected due to the disruption of chromosome pairing in prophase I. We found that this meiotic failure leads to a diminution in testicular size and a complete loss of ovarian structures. Our results show that normal Msh5 function is essential for meiotic progression and, in females, gonadal maintenance.

We isolated a mouse *Msh5* genomic clone and used it to construct a gene targeting vector (Fig. 1a) that was used to generate mice from two embryonic stem (ES) cell lines with the modified *Msh5* locus (Fig. 1b). These mice transmitted the modified locus

in a mendelian fashion, and we obtained viable *Msh5*^{-/-} mice. We failed to detect *Msh5* transcripts or Msh5 protein in testes of 24-day-old mice (Fig. 1d). These data suggest that the modified *Msh5* locus does not encode a functional Msh5 protein.

In mouse testis, the first meiotic wave begins at day 11 post-partum (pp; Fig. 2a), with prophase I commencing at day 13. *Msh5* is highly expressed in the gonads of humans¹⁹ and mice (Fig. 2a), and in the latter is coincident with the onset of the meiotic wave. *Msh5*^{-/-} males exhibited normal sexual behaviour, but were infertile due to the complete absence of epididymal spermatozoa. In contrast, *Msh5*^{+/-} males were fertile. Examination of seminiferous tubules in *Msh5*^{-/-} adult males revealed a disruption of spermatogenesis (Fig. 2b,c) causing a 70% reduction in testis size. Interstitial Leydig cells and tubular Sertoli cells are present in the mutant males, as are type A and B spermatogonia, but we observed no normal pachytene spermatocytes (Fig. 2d-g). At day 17 pp, the seminiferous epithelium of *Msh5*^{-/-} males is densely packed, although early signs of germ-cell loss are evident, both by reduced germ-cell nuclear antigen 1 (Gcna1; ref. 20) localization and increased apoptosis (Fig. 3a-d). By day 23 pp, tubules of wild-type mice contain round spermatids (data not shown). In contrast, elevated levels of

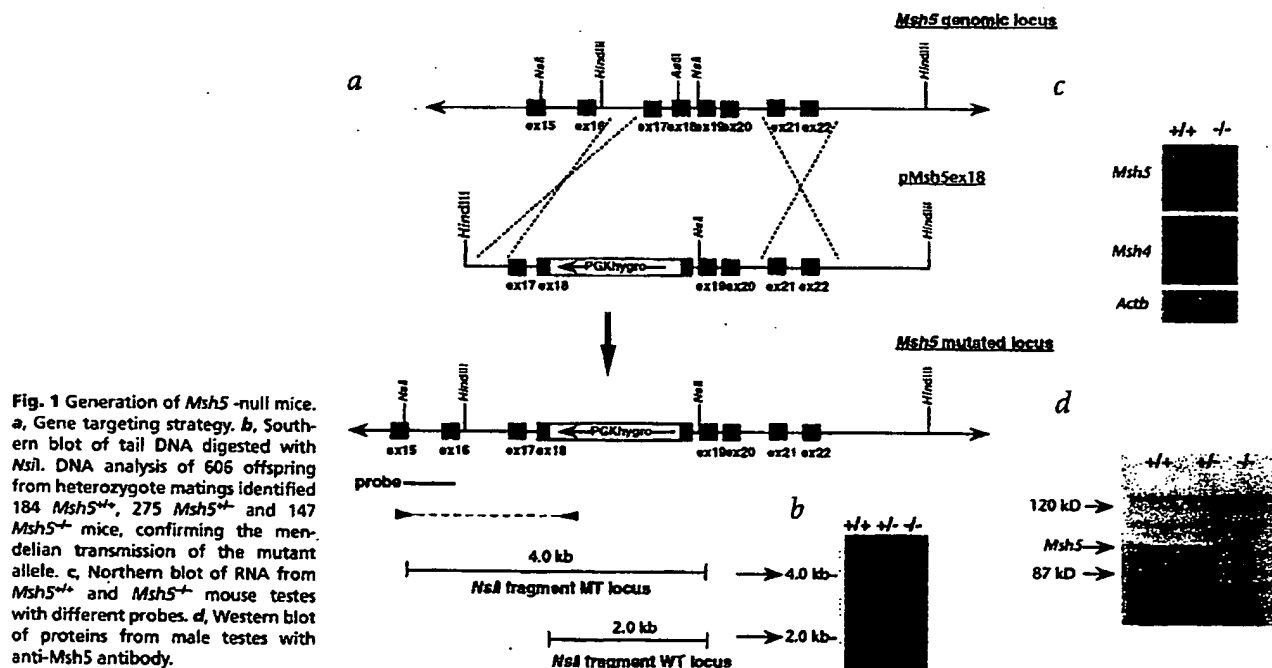


Fig. 1 Generation of *Msh5*-null mice. **a**, Gene targeting strategy. **b**, Southern blot of tail DNA digested with *NsiI*. DNA analysis of 606 offspring from heterozygote matings identified 184 *Msh5*^{+/+}, 275 *Msh5*^{+/-} and 147 *Msh5*^{-/-} mice, confirming the mendelian transmission of the mutant allele. **c**, Northern blot of RNA from *Msh5*^{+/+} and *Msh5*^{+/-} mouse testes with different probes. **d**, Western blot of proteins from male testes with anti-Msh5 antibody.

¹Department of Cell Biology, ²Department of Developmental and Molecular Biology, ³Department of Molecular Genetics, Albert Einstein College of Medicine, 1300 Morris Park Avenue, Bronx, New York 10461, USA. ⁴Dana Farber Cancer Institute, 44 Binney Street, Boston, Massachusetts 02115, USA. Correspondence should be addressed to W.E. (edelmann@aecom.yu.edu).

Letter

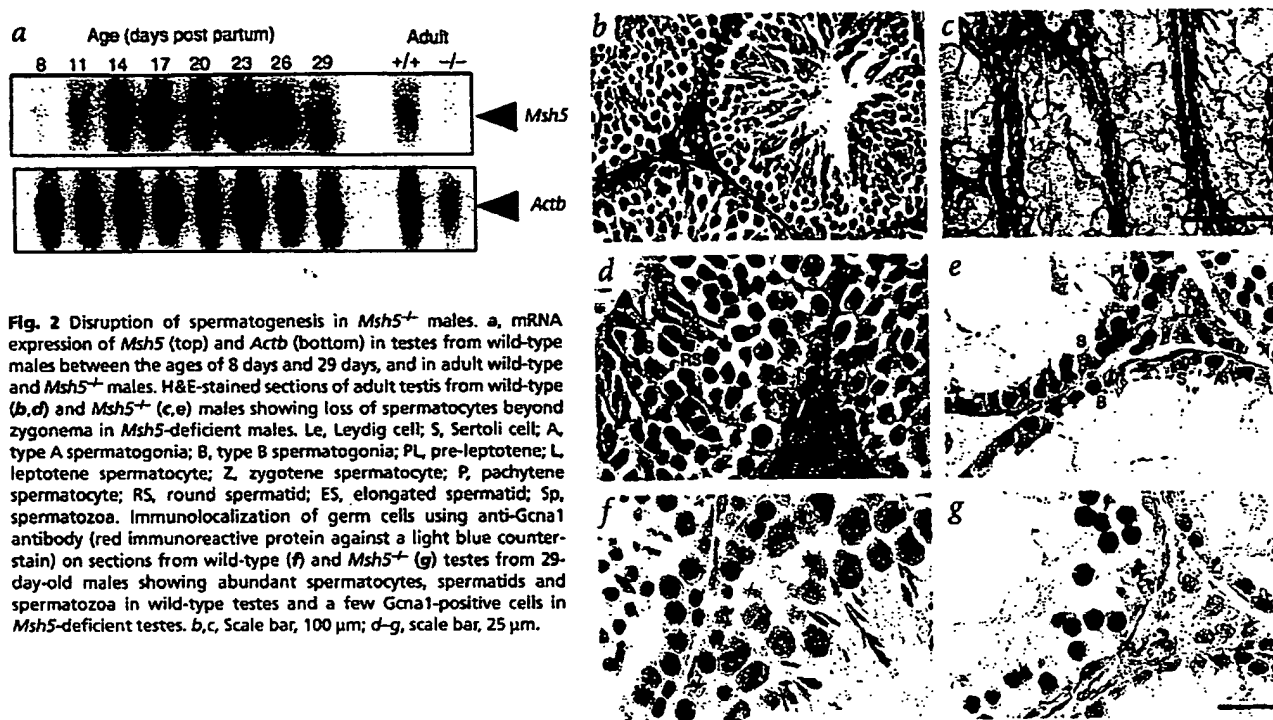


Fig. 2 Disruption of spermatogenesis in *Msh5*^{-/-} males. **a**, mRNA expression of *Msh5* (top) and *Actb* (bottom) in testes from wild-type males between the ages of 8 days and 29 days, and in adult wild-type and *Msh5*^{-/-} males. H&E-stained sections of adult testis from wild-type (**b,d,f**) and *Msh5*^{-/-} (**c,e,g**) males showing loss of spermatocytes beyond zygonema in *Msh5*-deficient males. Le, Leydig cell; S, Sertoli cell; A, type A spermatogonia; B, type B spermatogonia; PL, pre-leptotene; L, leptotene spermatocyte; Z, zygotene spermatocyte; P, pachytene spermatocyte; RS, round spermatid; ES, elongated spermatid; Sp, spermatozoa. Immunolocalization of germ cells using anti-Gcna1 antibody (red immunoreactive protein against a light blue counterstain) on sections from wild-type (**f**) and *Msh5*^{-/-} (**g**) testes from 29-day-old males showing abundant spermatocytes, spermatids and spermatozoa in wild-type testes and a few Gcna1-positive cells in *Msh5*-deficient testes. **b,c**, Scale bar, 100 μ m; **d-g**, scale bar, 25 μ m.

apoptosis in *Msh5*^{-/-} tubules leads to continued germ-cell attrition, and by adulthood almost the entire spermatogenic cell population is lost (Fig. 3e-h).

To analyse meiotic progression, we examined meiotic chromosome spreads at the light and electron microscope level. In 23-day-old wild-type spreads, silver staining revealed a range of chromosomal configurations, including those at leptotene, zygotene, pachytene and diplotene (Fig. 4a). In samples taken from four *Msh5*^{-/-} males of the same age, we found that 588 of 602 (97.7%) spermatocytes contained no synapsed chromosomes (Fig. 4b), compared to more than 92% of wild-type cells

(255/277) showing chromosomal configurations at zygotene and beyond. All of the spermatocytes from *Msh5*^{-/-} males contained univalent chromosomes and condensation levels corresponding to the zygotene and pachytene stages of meiosis. In the remaining 14 cells we observed only 29 partially paired chromosomes out of the expected 280 pairs (Fig. 4c). At least one-half of these (15/29) involved chromosomes of different lengths, suggesting that this pairing is non-homologous.

We examined the chromosomal association of Sycp1, Sycp3 (also known as Syn1 and Cor1, respectively) and Rad51, proteins known to be required for recombination and formation of the

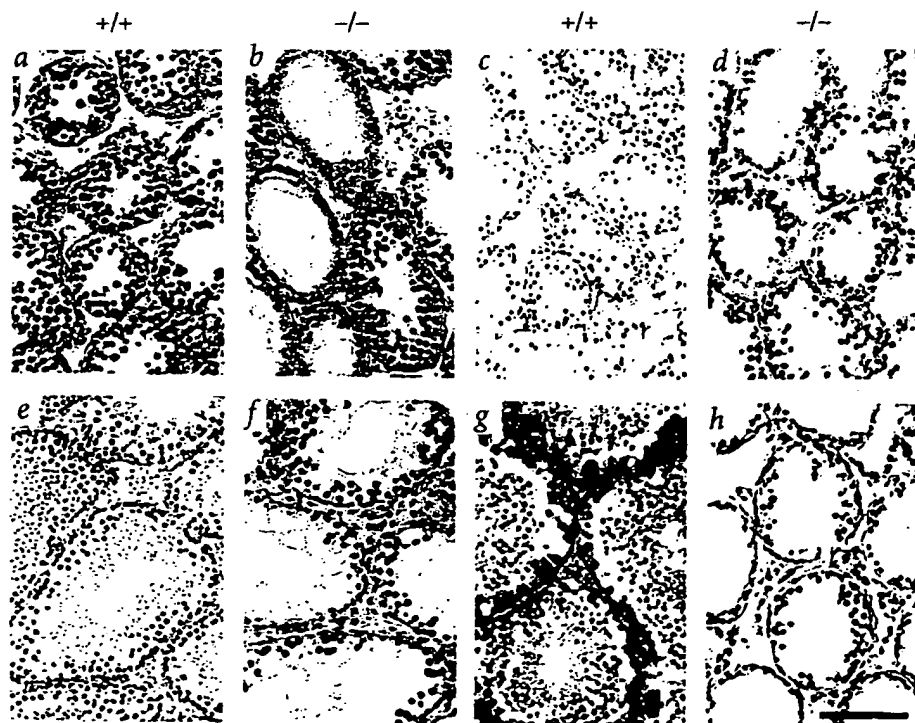


Fig. 3 Progressive depletion of germ cells in *Msh5*^{-/-} males during development. Germ-cell immunolocalization using anti-Gcna1 antibody in day 17 pp (**a-d**) and adult (**e-h**) of testes from wild-type (**a,e**) and *Msh5*^{-/-} (**b,f**) males, showing rapid depletion of germ cells from day 17 pp onwards in *Msh5*-deficient mice, in contrast with the increasing density and variety of spermatogenic cells in the seminiferous tubules of *Msh5*^{+/+} males. TUNEL staining of testes from wild-type (**c,g**) and *Msh5*^{-/-} males (**d,h**) showing continuous apoptosis from day 17 pp onwards, compared with the low level of apoptosis in tubules from wild-type males over the same time frame. Scale bar, 100 μ m.

Fig. 4 Disruption of meiosis before synapsis in *Msh5*^{-/-} spermatocytes. Silver-stained spermatocytes from wild-type (a) and *Msh5*^{-/-} (b, c) testes showing complete failure of pairing (b) or partial pairing (c) in the absence of *Msh5*. Arrowheads (c) indicate chromosomes showing partial pairing. Note that many of these chromosomes appear to be unequally paired. Immunofluorescent localization of Sycp1 and Sycp3 on synaptonemal complexes of wild-type pachytene spermatocytes (d) and axial elements of unsynapsed leptotene/zygotene spermatocytes from *Msh5*^{-/-} testes (e) is shown. Immunofluorescent localization of Rad51 on leptotene spermatocytes from wild-type (f) and *Msh5*^{-/-} males (g) is also shown.



synaptonemal complex^{21,22} (SC). Immunofluorescent localization of Sycp1 and Sycp3 on meiotic chromosomes using a combined antiserum demonstrated normal acquisition of SC in spermatocytes from wild-type males and identified pachytene spermatocytes as having 20 distinct condensed pairs of bivalents (Fig. 4d). In *Msh5*^{-/-} spermatocytes, all chromosomes were associated with the Sycp1/Sycp3 signal, indicating that axial element proteins accumulate along each chromosome (Fig. 4e), but no condensed bivalents were observed. In *Msh5*^{-/-} spermatocytes, Rad51 was localized in discrete foci along the univalent chromosomes (Fig. 4g), and the number and intensity of these foci appeared greater in the majority of *Msh5*^{-/-} cells than on leptotene or zygotene chromosomes from wild-type males (Fig. 4f) and did not decline as observed in wild-type spermatocytes, suggesting lack of progress towards pachytene. The presence of Rad51 on unsynapsed chromosomes from mutant mice suggests that meiosis is initiated and double strand breaks proceed in the absence of *Msh5*.

To examine the role of *Msh5* in female meiosis, we assessed ovarian function in *Msh5*^{-/-} adults. Mutants did not mate with wild-type males, nor did they undergo normal estrous cycles. *Msh5*^{-/-} females have normally structured oviducts and uteri but lack discernible ovaries (Fig. 5d, e). Instead, the ovarian bursa of *Msh5*^{-/-} females were empty or, more frequently, contained cystic structures with 1–4 cysts (Fig. 5e). At day 3 pp, ovaries of *Msh5*^{-/-} females contained fewer oocytes (Fig. 5a, b). By day 25 pp, the ovaries of *Msh5*^{-/-} females were reduced to a small

grouping of 1–3 follicles that appeared to be at post-antral stages of development and occasionally contained oocytes (Fig. 5c), whereas wild-type ovaries had abundant primordial follicles (not shown). The presence of oocytes in day 25 pp *Msh5*^{-/-} females was confirmed by RT-PCR detection of transcripts for the oocyte-specific protein, zona pellucida 3 (*Zp3*; ref. 23); however, in adults *Zp3* transcripts could only be detected in wild-type ovaries (Fig. 5f). Thus, the ovaries of *Msh5*^{-/-} females are normal in size at birth, but degenerate progressively to become

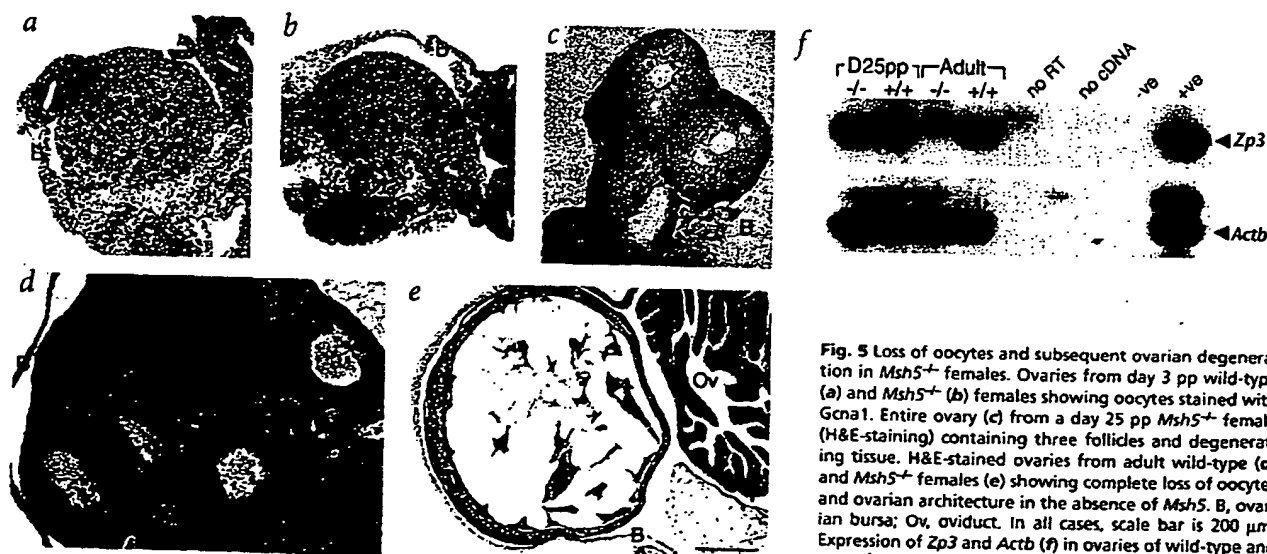
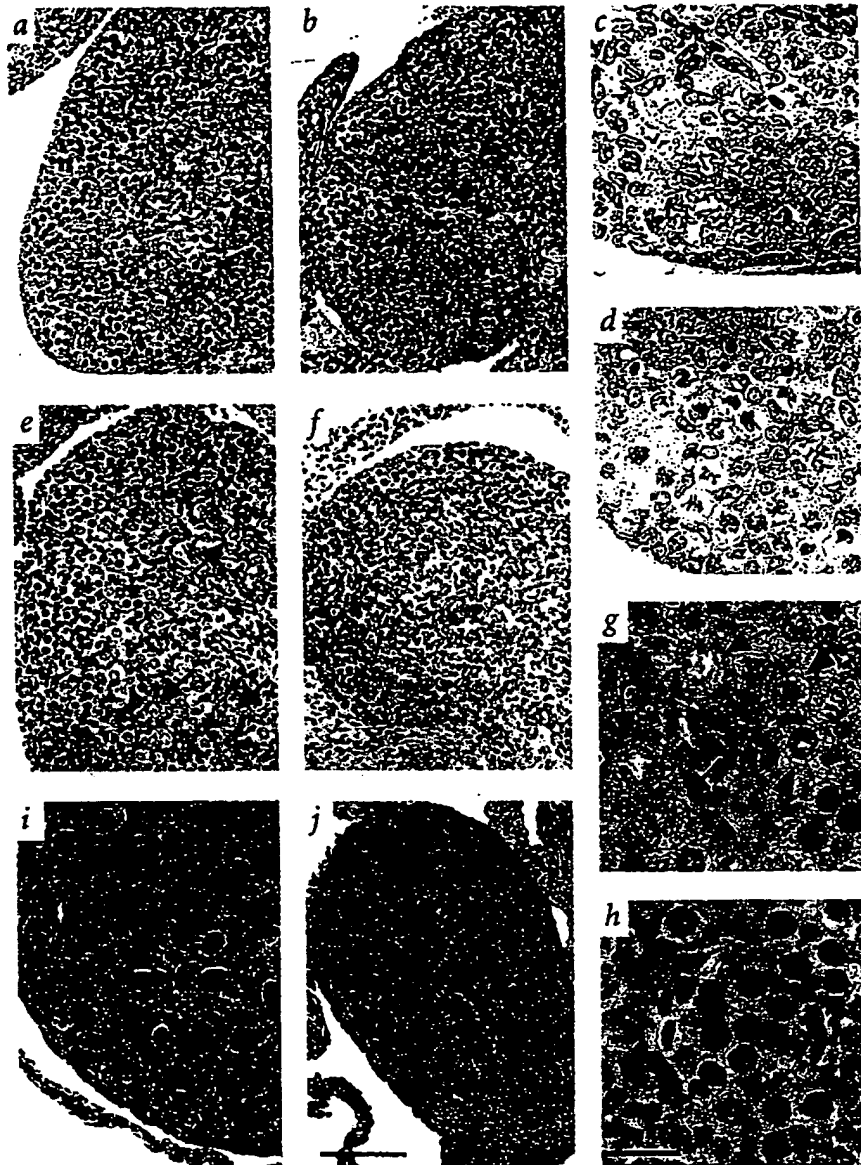


Fig. 5 Loss of oocytes and subsequent ovarian degeneration in *Msh5*^{-/-} females. Ovaries from day 3 pp wild-type (a) and *Msh5*^{-/-} (b) females showing oocytes stained with Gcnal. Entire ovary (c) from a day 25 pp *Msh5*^{-/-} female (H&E-staining) containing three follicles and degenerating tissue. H&E-stained ovaries from adult wild-type (d) and *Msh5*^{-/-} females (e) showing complete loss of oocytes and ovarian architecture in the absence of *Msh5*. B, ovarian bursa; Ov, oviduct. In all cases, scale bar is 200 μ m. Expression of *Zp3* and *Actb* (f) in ovaries of wild-type and *Msh5*^{-/-} ovaries on day 25 pp and in the adult.

letter

Fig. 6 Disruption of oogenesis in *Msh5*^{-/-} females leads to a failure of folliculogenesis. Ovaries from E18 wild-type (*a,c*) and *Msh5*^{-/-} (*b,d*) embryos showing oogonia stained with anti-Gcn1 (*a,b*) or H&E localization of meiotic chromosome detail (*c,d*). Gcn1 localization of oocytes in ovaries from day 3 pp wild-type (*e,g*) and *Msh5*^{-/-} (*f,h*) females is shown. Arrowheads indicate pachytene oocytes (punctate red staining of nucleus compared with solid red staining of pre-pachytene oocytes) and arrows indicate the appearance of the earliest primordial follicles. Gcn1 localization of oocytes in ovaries from day 6 pp wild-type (*i*) and *Msh5*^{-/-} (*j*) females (overstained to stain oocytes in meiotic arrest). Arrows indicate primordial follicles; arrowheads, oocytes. *a,b,e,f,i,j*, Scale bar, 100 μ m; *c,d,g,h*, scale bar, 25 μ m.



rudimentary, concomitant with the decline in oocyte numbers from before day 3 pp until adulthood.

We examined *Msh5* expression in wild-type ovaries by RT-PCR. *Msh5* expression was detected in embryonic day (E) 16, E18 and day 1 pp ovaries, coincident with the initiation of meiosis in females and consistent with the possibility that *Msh5* has a direct role in ovarian meiosis (data not shown). During late embryogenesis, ovaries of homozygous mutant females contain normal numbers of oocytes (Fig. 6*a-d*). Examination of H&E-stained sections revealed subtle differences in chromosome structure between wild-type and *Msh5*^{-/-} oocytes, characterized by clumping of nuclear contents in homozygous mutant oocytes (Fig. 6*d*) compared with readily identifiable chromosomes in wild-type oocytes (Fig. 6*c*). By day 3 pp, the number of oocytes in the ovaries of *Msh5*^{-/-} females was lower than that in wild-type ovaries (Fig. 6*e,f*) and did not exhibit the Gcn1 staining characteristic of pachytene oocytes (Fig. 6*g,h*). By day 6 pp, large primordial follicles containing readily identifiable oocytes were distributed throughout the ovaries of wild-type females (Fig. 6*i*), whereas the oocyte pool was diminished in ovaries from *Msh5*^{-/-} females (Fig. 6*j*).

Our results show that *Msh5* is required for chromosome pairing and/or synapsis. Mice mutated in other mutHLS genes (*Pms2* and *Mlh1*) that interact with MSH homologues are also sterile due to meiotic abnormalities; however, meiosis is aberrant at a different stage in these mice. In *Pms2*^{-/-} mice, chromosome pairing is disrupted, but spermatids and spermatozoa, although abnormal, are observed¹². In *Mlh1*^{-/-} mice, normal pairing is detected but post-pachytene meiotic stages are rarely observed^{13,14}. These results suggest that these proteins have distinct roles at different stages of meiosis in mice.

In adult *Msh5*^{-/-} females, we observe a complete loss of ovarian structures. Similar to *Msh5*^{-/-} males, germ cells populate the genital ridge but oocytes never progress beyond zygotene. The progressive loss of oocytes from E18 appears to result from meiotic failure and activation of a checkpoint resulting in apoptosis, as seen in *Msh5*^{-/-} spermatocytes. This results in almost complete absence of oocytes by day 6 pp, and the ovary begins to degenerate such that, in the adult, it is usually entirely absent or consists of a few large cysts. The degenerating oocytes fail to initiate folliculogenesis, indicating that there must be dialogue between the oocyte

and surrounding stroma for this process as well as maintenance of ovarian morphology. The phenotype of *Msh5*^{-/-} females differs from that seen in *Dmclh*^{-/-} mice, which also show a failure of pairing/synapsis and oocyte loss in early neonatal life but retain at least a rudimentary ovary in adulthood^{24,25}. These differences suggest that either the requirement for *Msh5* is slightly earlier than *Dmclh* or there is partial redundancy for *Dmclh* function.

There are similarities in the ovarian phenotype in female *Msh5*^{-/-} mice and Turner syndrome patients^{26,27}. In both cases, rapid loss of oocytes is seen during intrauterine and neonatal life and consequent ovarian degeneration. It is possible that the failure of homologous chromosome pairing, whether at the level of the X chromosome (as in Turner patients) or throughout the entire chromosome population (as in *Msh5*^{-/-} oocytes), triggers an apoptotic checkpoint that ultimately results in complete ovarian degeneration.

Methods

***Msh5* cDNA cloning.** The original segment of *Msh5* was obtained by PCR using BALB/c genomic DNA (Clontech) and primers (5'-GTG-CTGTGGAATTCAGGATAC-3', sense; 5'-CCAGAACTCTCTGGA-GAAGC-3', antisense) based on human cDNA sequence. The remainder

of the *Msh5* coding sequence was cloned by RT-PCR using the Advantage cDNA PCR kit and gene-specific primers 5'-CTCCACTATC-CACITTCATGCCAGATGC-3' (sense) and 5'-GCTGGGGAGGAGCACTGGAAGGACTCTCA-3' (antisense, based on human 3' untranslated cDNA sequence). The mouse *Msh5* genomic locus was cloned from a P1 mouse ES cell genomic library (Genome Systems) that yielded three clones: 11051, 11052 and 11053.

Construction of the pMsh5ex18 targeting vectors. A genomic *Msh5* fragment containing exon 18 was obtained by screening a mouse genomic Charon 35, 129/Ola phage library. A 3.8-kb *HindIII* fragment containing exon 18 was subcloned into pBluescript SK+/- and a 2.0-kb *BglII* PGKhygro cassette was cloned into the *AatII* site at codon 528 in exon 18 using *BglII/AatII* adaptors. The resulting gene targeting clone was designated pMsh5ex18.

Electroporation of ES cells. The targeting vector pMsh5ex18 (50 µg) was electroporated into WW6 ES cells²⁸ and hygromycin-resistant colonies were isolated and screened by PCR using forward primer A, 5'-AGCTG-GAGAACTGGACTCTC-3', and reverse primer B, 5'-TGGAAGGATTG-GAGCTACGG-3'. Positive ES cell colonies were identified by a 1.5-kb PCR fragment specific for the targeting event. Six positive cell lines, MSH5-1, MSH5-33, MSH5-41, MSH5-52, MSH5-58 and MSH5-109, were identified and the correct targeting event was shown by *NsiI* digestion of high molecular weight DNA and Southern-blot analysis using a 0.8-kb *EcoRI/HindIII* probe directed at the 5' intron region between exons 13 and 14 not included in the targeting vector.

Northern-blot analysis. Poly(A) RNA (4 µg) from 24-day-old males was separated on 1.0% agarose formaldehyde gels, transferred to nitrocellulose membrane and hybridized with an *Msh5* probe corresponding to exons 3-8, a probe spanning the complete mouse *Msh4* cDNA and a human *Actb* (β-actin) probe.

Western-blot analysis. Equal amounts of protein from testes extracts of 23-day-old males were separated on a 10% SDS-PAGE gel and transferred onto an Immobilon-P (Millipore) membrane. The membrane was blocked in TBS, 0.1% Tween-20, 5% nonfat dry milk and 10% goat serum (Sigma) and incubated with primary anti-Msh5 antibody (1:1,000). Bound protein was detected by chemiluminescence using goat anti-mouse IgG horseradish peroxidase conjugate (1:30,000; Sigma).

Histology. Ovaries from *Msh5*^{+/+} and *Msh5*^{-/-} females between E18 and 5 weeks pp were removed and fixed in Bouins or 4% buffered formalin for 30-360 min before transfer to 70% ethanol. Testes were fixed by transcardiac perfusion of 4% buffered formalin and then overnight in fresh fixative. All tissues were processed for histology by routine methods and sectioned (3 or 5 µm).

Chromosomes. Chromosome spreads were prepared as described²⁹ with modifications. Spreads were then either silver-stained in 50% silver nitrate at 65 °C for 6 h (for electron microscopy) or subjected to immunofluorescent localization of chromosomally associated proteins³⁰.

Acknowledgements

We thank the following colleagues for generously providing antibodies and advice: P. Moens, B. Spyropoulos and G. Enders. The expert technical assistance of H. Hou Jr, L. Zhu and members of the AECOM Analytical Imaging Facility (F. Maculoso, L. Gunther and C. Marks) is appreciated. We also thank S. Shenoy for training and help with the CCD imaging system. This work was supported by NIH grants (CA 76329 to W.E.; CA 67944 and NO1-CN-65031 to R.K.; CA 44704 to R.D.K.), the American Cancer Society (R.K.) and a Cancer Center grant to AECOM (CA13330).

Received 15 August 1998; accepted 24 November 1998.

- Modrich, P. & Lahue, R. Mismatch repair in replication fidelity, genetic recombination and cancer biology. *Annu. Rev. Biochem.* 65, 101-133 (1996).
- Kolodner, R. Biochemistry and genetics of eukaryotic mismatch repair. *Genes Dev.* 10, 1433-1442 (1996).
- Fishel, R.A. et al. The human mutator gene homolog MSH2 and its association with hereditary nonpolyposis colon cancer. *Cell* 75, 1027-1038 (1993).
- Leach, F.S. et al. Mutations of a mutS homolog in hereditary nonpolyposis colorectal cancer. *Cell* 75, 1215-1225 (1993).
- Bronner, C.E. et al. Mutation in the DNA mismatch repair gene homologous *hMLH1* is associated with hereditary nonpolyposis colon cancer. *Nature* 368, 258-261 (1994).
- Papadopoulos, N. et al. Mutation of a *mutL* homolog in hereditary colon cancer. *Science* 263, 1625-1629 (1994).
- Akiyama, Y. et al. Germ-line mutation of the hMSH6/GTBP gene in an atypical hereditary nonpolyposis colorectal cancer kindred. *Cancer Res.* 57, 3920-3923 (1997).
- Miyaki, M. et al. Germline mutation of *MSH6* as the cause of hereditary nonpolyposis colorectal cancer. *Nature Genet.* 17, 271-272 (1997).
- de Wind, N., Dekker, M., Berns, A., Radman, M. & te Riele, H. Inactivation of the mouse *Msh2* gene results in mismatch repair deficiency, methylation tolerance, hyperrecombination, and predisposition to cancer. *Cell* 82, 321-330 (1995).
- Reitmair, A.H. et al. *MSH2*-deficient mice are viable and susceptible to lymphoid tumours. *Nature Genet.* 11, 64-70 (1995).
- Edelmann, W. et al. Mutation in the mismatch repair gene *Msh6* causes cancer susceptibility. *Cell* 91, 467-477 (1997).
- Baker, S.M. et al. Male mice defective in the DNA mismatch repair gene *Pms2* exhibit abnormal chromosome synapsis in meiosis. *Cell* 82, 309-320 (1995).
- Edelmann, W. et al. Meiotic pachytene arrest in *MLH1*-deficient mice. *Cell* 85, 1125-1134 (1996).
- Baker, S.M. et al. Involvement of mouse *Mlh1* in DNA mismatch repair and meiotic crossing over. *Nature Genet.* 13, 336-342 (1996).
- Hollingsworth, N.M., Ponte, L. & Halsey, C. *Msh5*, a novel mutS homolog, facilitates meiotic reciprocal recombination between homologs in *Saccharomyces cerevisiae* but not mismatch repair. *Genes Dev.* 9, 1728-1739 (1995).
- Ross-Macdonald, P. & Roeder, G.S. Mutation of a meiosis-specific MutS homolog decreases crossing over but not mismatch correction. *Cell* 79, 1069-1080 (1994).
- Prolla, T.A., Christie, D.M. & Liskay, R.M. Dual requirement in yeast DNA mismatch repair for *MLH1* and *PMST*, two homologs of the bacterial *MutL* gene. *Mol. Cell. Biol.* 14, 407-415 (1994).
- Plug, A.W. et al. Changes in protein composition of meiotic nodules during mammalian meiosis. *J. Cell Science* 111, 413-423 (1998).
- Winand, N.J., Panzer, J.A. & Kolodner, R.D. Cloning and characterization of the human and *C. elegans* homologs of the *Saccharomyces cerevisiae Msh5* gene. *Genomics* 53, 69-80 (1998).
- Enders, G.C. & May, J.J. Developmentally regulated expression of a mouse germ cell nuclear antigen examined from embryonic day 11 to adult in male and female mice. *Dev. Biol.* 163, 331-340 (1994).
- Moens, P.B., Pearlman, R.E., Traut, W. & Heng, H.H. Chromosome cores and chromatin at meiotic prophase. *Curr. Top. Dev. Biol.* 37, 241-263 (1998).
- Plug, A.W., Xu, J., Reddy, G., Golub, E.I. & Ashley, T. Presynaptic association of Rad51 protein with selected sites in meiotic chromatin. *Proc. Natl Acad. Sci. USA* 93, 5920-5924 (1996).
- Wassarman, P.M. Zona pellucida glycoproteins. *Annu. Rev. Biochem.* 57, 415-442 (1988).
- Yoshida, K. et al. The mouse RecA-like gene *Dmc1* is required for homologous chromosome synapsis during meiosis. *Mol. Cell* 1, 707-718 (1998).
- Pittman, D.L. et al. Meiotic prophase arrest with failure of chromosome synapsis in mice deficient for *Dmc1*, a germline-specific RecA homolog. *Mol. Cell* 1, 697-705 (1998).
- Singh, R.P. & Carr, D.H. The anatomy and histology of XO human embryos and fetuses. *Anat. Rec.* 155, 369 (1966).
- McDonough, P.G. Gonadal dysgenesis and its variants. *Pediatr. Clin. North Am.* 19, 631-652 (1972).
- Ioffe, E. et al. WW6: An embryonic stem cell line with an inert genetic marker that can be traced in chimeras. *Proc. Natl Acad. Sci. USA* 92, 7357-7361 (1995).
- Counce, S.J. & Meyer, G.F. Differentiation of the synaptonemal complex and the kinetochore in *Locust* spermatocytes studied by whole mount electron microscopy. *Chromosoma* 44, 231-253 (1973).
- Spyropoulos, B. & Moens, P.B. *In situ* hybridization of meiotic prophase chromosomes. *Methods Mol. Biol.* 33, 131-139 (1994).